Mesostructured SiO_2-doped TiO_2 with enhanced thermal stability prepared by a soft-templating sol-gel route

Guillermo Calleja*, David P. Serrano, Raúl Sanz and Patricia Pizarro

Department of Chemical and Environmental Technology,

ESCET, Universidad Rey Juan Carlos, c/ Tulipán s/n, 28933, Móstoles, Madrid, Spain

Published on:

Microporous and Mesoporous Materials 111 (2008) 429–440

Doi: http://dx.doi.org/10.1016/j.micromeso.2007.08.021

*Corresponding author. Tel. +34 91 488 7006: Fax: +34 91 488 7068; E-mail address: guillermo.calleja@urjc.es

Abstract

Mesostructured SiO_2-TiO_2 mixed oxides have been prepared by a soft-templating sol-gel route, using a non-ionic triblock copolymer as structure directing agent. Tetraethylorthosilicate (TEOS) and titanium tetraisopropoxide (TTIP) have been employed as Si and Ti sources, respectively. Using a prehydrolysis TEOS step allows mixed oxides to be produced with a homogeneous porosity and with no phase segregation, in a wide range of Si/Ti compositions. Both the hydrolysis molar ratio and the silicon content have been found to be important factors determining the final properties of these materials. For instance, mixed oxides containing low silicon concentrations exhibit N_2 physisorption isotherms typical of mesoporous materials, although with an important contribution of microporosity. On the other hand, increasing the hydrolysis molar ratio makes more difficult to reach a total dispersion of SiO_2 through the TiO_2 matrix. Even with low SiO_2 loadings, the thermal stability is effectively enhanced, when compared to the equivalent pure TiO_2 materials, as a consequence of a delay in the titania crystallization to anatase. Thus, after calcination at 300 ºC for 3 h, mixed oxides containing low Si/Ti ratios ($\leq$ 20) show BET surface area in the range 290-346 m^2/g, while pure TiO_2 materials largely collapse under the same treatment and their BET surface area drop strongly to values around 125 m^2/g. This synthesis route, therefore, provides mesoporous TiO_2-rich materials with enhanced stability and textural properties, which is of high interest for applications as catalysts and supports.

Keywords

Soft-templating, mixed oxides, mesoscopic order, SiO_2-doped TiO_2, thermal stability.

1. Introduction

High temperature applications of porous TiO_2, prepared by either wet methods or sol-gel routes, are hindered by the low thermal stability usually exhibited by these materials. This lack of thermal stability is originated by the phase transformations of titania particles from amorphous to anatase and, subsequently, from anatase to rutile. Depending on the synthesis conditions, temperature ranges in which these transformations may occur are quite wide, but they are always associated with structural and porosity damages. This effect is more pronounced when anatase to rutile transition takes place, since it is accompanied by a drastic change in the crystal size, as well as by a collapse of the porous structure due to a sinterization process [1] [2]. Therefore, in order to improve the thermal stability of porous titania materials, the above mentioned transformations must be avoided or delayed.

One widespread route to hinder crystallographic transitions of TiO_2 is the incorporation of another inorganic oxide, which either increases the activation energy of the nucleation process or reduces the number of nucleation active sites. Nowadays, many inorganic oxides, such as WO_3, MnO_2, CuO, V_2O_5, SiO_2, Al_2O_3, have been incorporated into TiO_2 materials with the purpose of providing appropriate features for specific applications [3-7]. Kim et al. [3] studied the effect of three dopants (Al, Si and Zr) on the stability of TiO_2 exhibiting bimodal porosity. Using a synthesis method based on the co-precipitation of the corresponding organometallic precursors, the authors introduced dopant concentrations ranging from 5 to 40 mol %. Among their results, it is remarkable that such dopants not only delayed the anatase-rutile phase transition, but they caused also a smaller growth of anatase crystals. This effect was more intense when increasing the dopant concentration, the effectiveness on the thermal stabilization being higher in

the order Zr > Si > Al. Moreover, after calcination, doped materials preserved higher textural properties due to a slower phase transition and to a lower sinterization effect. In particular for the SiO_2-TiO_2 systems, their benefits arise from a combination of a better thermal stability and mechanical strength, both properties provided by silica, and good optical and catalytic properties, given by the TiO_2 phase.

SiO_2-TiO_2 materials are used in very different fields [8], such as protective coatings for stainless steel, antireflection coatings for optical glasses or, even, for the preparation of glasses having extremely low thermal expansion coefficients and high refraction indexes. Likewise, one of the major interests is focused on the development of either catalysts or supports where the properties provided by the combination of both inorganic phases can be exploited. Among these properties, the following deserve to be mentioned: a) enhanced photocatalytic properties [9]; b) acidity, making these materials good acid catalysts for a number of reactions [10] and c) high thermal and mechanical stability [8].

Several methods have been reported on the preparation of SiO_2-TiO_2 mixed oxides: mixing particles of both preformed oxides [11], covering silica supports with titania films [12], attaching TiO_2 onto mesoporous silica [13], flame co-hydrolysis of $TiCl_4$ and $SiCl_4$ vapours [14] and either hydrothermal co-precipitation or co-gelation from the corresponding titania and silica precursors [15]. Among all these alternatives, sol-gel techniques couple reproducibility and flexibility with other advantages related to the properties of the final material, such as a high microscopic structural homogeneity, with the heteroatoms integrated in the same inorganic matrix.

In this way, a variety of works have reported the sol-gel synthesis of SiO_2-TiO_2 mixed oxides with Si/Ti ratios equal to or higher than 1/1 [13-17], whereas several studies for

Ti rich-mixed oxides [3,9,18-20] have also been published. However, the synthesis of ordered mesoporous silica-doped titania by the sol-gel route in the presence of a surfactant as structure-directing agent has been hardly investigated. These last materials are very promising in fields such as heterogeneous photocatalysis, since they could provide simultaneously enhanced photocatalytic and thermal properties. Ordered mesoporous inorganic oxides synthesized in the presence of a surfactant are characterized by having higher surface areas and particle sizes, as well as a narrow mesopore size distribution. For TiO_2-based materials, these properties are expected to improve the process of dye deposition (in order to shift the photoactivity to the visible spectra) and to facilitate their recovery, in the case of liquid-phase photocatalytic applications.

In this field, we have previously published the preparation of mesoporous pure titania exhibiting high surface area (up to 582 m^2/g) by using a sol-gel route in the presence of a non ionic triblock copolymer as soft-template [21,22]. Nevertheless, the thermal stability of such xerogels is low, the pore structure being seriously damaged under mild calcination conditions. Other methods have been investigated for the synthesis of mesostructured TiO_2 [23,24] but, when prepared in the pure titania form, thermal stability is again the usual and main drawback of such materials.

In the present work, the synthesis of SiO_2-doped mesoporous TiO_2 by the sol-gel route, using a non-ionic triblock copolymer surfactant (Pluronic P-123) as template, has been investigated. The main goals of this paper were: i) to study the effect of SiO_2 concentration on the final properties of mesoporous TiO_2 synthesized with different hydrolysis molar ratios and ii) to evaluate the thermal stability of the SiO_2-TiO_2 mixed oxides.

2. Experimental section

2.1 Sample preparation

Mesostructured SiO_2-TiO_2 mixed oxides were synthesized via a soft templating sol-gel route using tetraethylorthosilicate [TEOS, $Si(OC_2H_5)_4$, Aldrich ≥ 98%] as silica precursor, titanium tetraisopropoxide [TTIP, $Ti(OCH(CH_3)_2)_4$, Alfa Aesar ≥ 97%] as titania source and poly(ethylenglycol) - block- poly(propylenglycol) - block - poly(ethylenglycol) [$PEO_{20}PPO_{70}PEO_{20}$, Pluronic P-123, Aldrich], as non-ionic surfactant. All reactants were used as received.

Since the hydrolysis rates of TEOS and TTIP are quite different, the former was prehydrolyzed in order to ensure a homogeneous SiO_2 dispersion into the titania framework during the synthesis reactions. Thus, initially 5 g of Pluronic were dissolved in 24 g of 2-propanol (*i*-PrOH) containing 0.8 M HCl. Once the surfactant was dissolved, the required amount of TEOS was added and stirred at 40ºC for 1 h. At the same time, a solution of TTIP in 79 g of 2-propanol was preheated at 40ºC during 30 min. Subsequently, the solution containing both Pluronic and hydrolyzed TEOS was slowly added to the titania precursor solution under vigorous stirring. Once the gel was formed, the stirring was stopped and the system was aged at the same temperature (40ºC) so that the total synthesis time was 20 h. The gel was then dried under vacuum at room temperature and the xerogel so obtained was washed twice with 50 ml of ethanol, dried again under vacuum and ground to obtain a fine powder.

The initial molar composition of the synthesis was as follows: 1 (TTIP+TEOS) : 0.017 P-123: 34 *i*-PrOH : X H_2O: Y HCl.

The surfactant was effectively removed by solvent extraction during 24 h, using 100 ml of boiling ethanol per 1.5 g of solid. The final solid products were named as SiTi-HX-Z, where *X* denotes the value of H, that is, the hydrolysis molar ratio [H=mol H_2O/mol(Ti+Si)] employed and *Z* indicates the molar Si/(Ti+Si) percentage.

Calcinations were performed at 300 ºC for 3 hours, using a heating rate of 1.8 ºC/min, under static air. Calcined samples were identified by adding a "*C*" at the end of their labels. For example, SiTi-H3-10C means that this material was prepared under the following conditions: hydrolysis molar ratio H = 3, Si/Ti molar ratio = 10/90, extraction of surfactant with boiling ethanol and, finally, calcination at 300 ºC.

2.2 Characterization

Powder X-ray diffraction (XRD) analyses were carried out using a Philips X´PERT MPD diffractometer operating with CuKα radiation. For low angle determinations, a step size of 0.03º with a step time of 5 s was used, the 2θ angle range being 0.5-5º. Wide-angle patterns were recorded from 2θ = 20º to 35º, using a step size of 0.1º and a step time of 5 s. For determinations of crystallinity evolution as a function of temperature, a high-temperature chamber was installed into the diffractometer, operating under a nitrogen flow. Once the desired temperature was reached, and after 15 minutes of stabilization at such temperature, the wide-angle diffractogram was registered.

DR-UV/Vis spectra were obtained in a Varian Cary 500 Scan UV-VIS-NIR instrument, the signal being registered as Kubelka-Munk function [F(R)]. Band-gap was calculated assuming the proportionality existing between F(R) and the absorption coefficient (σ) [25,26], using the initial absorption branch of the spectra.

Nitrogen adsorption-desorption isotherms at -196 °C were obtained on a Micromeritics Tristar 3000 sorptometer. Previously, the samples were degassed at 120 ºC under nitrogen. The surface area was determined using the Brunauer-Emmet-Teller (BET) equation. The pore size distribution was obtained applying the Barret-Joyner-Halenda (BJH) model to the adsorption branch of the isotherm. Micropore volume was estimated by the t-plot method with the Harkins and Jura model.

A Philips Technai 20 Transmission Electron Microscope, operating with a tungsten filament working at 200 kV, was used to obtain TEM images. Microscopic chemical composition of the samples was determined by EDX technique. For this purpose, regions below 0.1 μm^2 corresponding to different and thin particles were analyzed.

Ti content of the mixed oxides was determined by ICP technique using a Varian Vista AX Axial CCD Simultaneous ICP-AES spectrometer. The wavelength selected for Ti analysis was 336.22 nm. Previously to the analyses, samples were processed by an acid digestion treatment.

3. Results and discussion

SiO_2-TiO_2 mixed oxides were synthesized by a sol-gel route in the presence of a surfactant with the aim to obtain ordered mesoporous solids. The role of both the silicon content and/or the hydrolysis molar ratio during the synthesis reactions and their effect on the final properties of these materials was evaluated. Subsequently, the thermal stability of these properties was also investigated.

3.1 Properties of SiO_2-TiO_2 materials after surfactant removal

Both the hydrolysis molar ratio (H) and the silicon content were expected to affect strongly the gelation time of the synthesis mixture and, consequently, the final

properties of the materials so obtained. For sol-gel methods, it is well known that the higher the water amount existing in the synthesis solution, the faster the hydrolysis and condensation reactions of the initial alkoxide precursors [21]. In addition, for syntheses based on soft-templating routes, incorporation of water has two other crucial roles: it determines the type of metallic center-surfactant interactions and it facilitates the arrangement of surfactant molecules into well ordered micelles, which will serve as template to form the inorganic oxide structure. On the other hand, both oxidation state and coordination number of silicon in TEOS precursor is 4, so that it exhibits a low trend to increase its coordination. This fact, together with a higher electronegativity and lower partial charge of Si^{4+} than Ti^{4+} (both cations existing as alkoxydes) derive in a much lower sensitivity of the former cation to the hydrolysis reactions.

Table 1 illustrates the gelation times observed for the samples synthesized using different hydrolysis molar ratios and/or silicon contents. Concerning the series of materials prepared with H = 3, low concentrations of Si led to almost the same gelation times as for pure TiO_2 materials (> 6 hours), while by using equimolar amounts of Si and Ti, the gelation time was reduced to less than 3 hours. The hydrolysis molar ratio relative to the TiO_2 precursor (mol H_2O/mol TTIP) is 3 for the pure TiO_2 sample preparation, while it increases to 6 for SiTi-H3-50. Since the water amount available to hydrolyze the Ti precursor is twice for the later sample, it seems quite reasonable to have a strong reduction of gelation time. On the other hand, when the synthesis was carried out using a Si/Ti ratio of 70/30, more than 10 hours were needed to observe the gel formation. Silicon is now the predominant atom and its lower reactivity with water accounts for this last behaviour.

By increasing the total hydrolysis molar ratio to 6, gelation times were reduced up to around 4 minutes when molar Si/Ti ratios equal to or below 50/50 were used. However, the increase of silicon content to Si/Ti = 70/30 delayed the gel formation to 5 hours. For the synthesis carried out with H = 10, a white gel appeared in the following times: immediately, for the samples prepared with Si/Ti ≤ 20/80; before 1 minute, for Si/Ti = 50/50 and after 1 hour, for Si/Ti = 70/30. In addition, using this last water amount, a pure SiO_2 material was obtained although no gelation process was detected, but a white bulky suspension was formed.

Table 2 summarizes the main textural properties of SiO_2-TiO_2 mixed oxides prepared using different hydrolysis molar ratios and/or silicon contents. A general trend can be observed consisting in a BET surface area increase with the silicon content, as long as the relative molar H_2O/Si ratio is over 50. However, when the amount of water available to hydrolyze the silicon precursor is below that value, materials with lower porosity are produced. Thus, BET surface areas of 582, 437 and 515 m^2/g are obtained for samples SiTi-H3-5, SiTi-H6-10 and SiTi-H10-20, respectively, but this parameter decreases to 98, 231 and 276 m^2/g for SiTi-H3-50, SiTi-H6-50 and SiTi-H10-70, respectively. Total pore volumes achieved for these last three xerogels reach also the lowest values of 0.036, 0.094 and 0.113 cm^3/g, respectively. A new increase of BET surface area occurred for the largest Si concentrations, which is attributed to the formation of a different class of material with SiO_2 as predominant phase. In the case of the syntheses carried out with hydrolysis molar ratios of 3 and 6, this last effect appeared for the samples containing a Si/Ti ratio = 70/30. However, for the syntheses with H = 10, the increase of S_{BET} occurred just for the pure SiO_2 material.

On the other hand, the mean pore diameter, estimated by applying the BJH model to the adsorption branch of the isotherm, decreases progressively as the silicon content is enlarged for the three series of samples, denoting the progressive transition to a different porous material induced by a higher influence of the silicon chemistry on the synthesis reactions.

N_2 adsorption-desorption isotherms corresponding to the series of materials prepared with hydrolysis molar ratio H = 3 are illustrated in Figure 1 (A). A progressive change from isotherms close to type IV (typical of mesoporous materials, according to IUPAC classification), to other essentially of type I (corresponding to microporous samples) can be clearly observed. BJH pore size distribution (Figure 1(B)) shows that the nitrogen uptake of samples prepared with Si/Ti ratios below 50/50 occurs in a quite narrow range of pore diameters, located in the mesopore region, with the maximum shifting to lower pore sizes as the Si content is higher. An adsorption branch at low pore diameters appears in all cases, denoting the additional existence of micropores, this adsorption being more pronounced at higher silicon loadings. The contribution of microporosity for the samples prepared with Si/Ti ratios < 50/50 is verified by the t-plot estimation of micropore volume (V_{MIC}), as shown in Table 2. Finally, syntheses using higher Si/Ti ratios led to microporous materials.

Although it is not shown here, it must be mentioned that samples prepared using H = 6 exhibit isotherms typical of mesoporous materials, with the exception of SiTi-H6-50, which is essentially microporous. This later material, indeed, represents the transition of mixed oxides with a TiO_2 matrix, to another one which is mainly siliceous. An important adsorption at low relative pressures can also be appreciated for the mesoporous samples, indicating a contribution of microporosity (Table 2). BJH pore

size distribution of these samples, obtained from the adsorption branch of the isotherms, show a relatively high uniformity on the pore diameter, except for SiTi-H6-5, which exhibits a pore size distribution close to bimodal (Table 2). In the case of the materials synthesized using H = 10, a clear evolution from type IV isotherms to others of type I is produced as the Si/Ti molar ratio is increased (Table 2). With the exception of SiTi-H10-5, BJH pore size distributions corresponding to the solids showing type IV isotherms (Si/Ti ≤ 20) are quite narrow, with the maximum centred in the mesoporous range (Table 2). As for the last batch of samples, the sample containing a molar Si/Ti ratio = 5 exhibits a broad pore size distribution, close to bimodal, which could be considered as the transition between the porous properties of pure TiO_2 and SiTi-H10-10.

Dutoit et al. have reported the preparation of mixed TiO_2-SiO_2 aerogels consisting in Ti atoms highly dispersed into the silica matrix. They employed a sol-gel route in absence of surfactants, with silicon tetramethoxide and titanium tetraisopropoxide modified with acetylacetonate as Si and Ti sources, respectively [27]. These authors found that, with a prehydrolysis of the Si precursor, lower concentrations of titanium led to higher microporosity and lower BET surface areas. Moreover, Klein et al., using synthesis conditions close to those here reported for SiO_2-rich samples (H_2O/Ti+Si = 2, Si/Ti = 67/3, HCl/Ti+Si = 0.35), but without the presence of a surfactant, obtained also similar textural properties: S_{BET} = 300 m^2/g, d_{PORE} = 0.75 nm and V_{MIC} = 0.11 cm^3/g [28].

Wide-angle XRD analysis (not shown here) revealed an essentially amorphous character of all these materials. However, in the low-angle XRD patterns (Figure 2) of the TiO_2-rich mixed oxides (Si/Ti < 50/50) prepared using H = 3 and 6, a broad diffraction peak (100) appears, which shows the presence of some periodic arrangement in the pore

structure. The intensity of this diffraction signal decreases as the silicon amount is higher and practically disappears when Si/Ti ≥ 50/50 is employed, indicating an enhancement of the mesoscopic order when low concentrations of silicon are included into the titania structure. Mixed oxides obtained from H = 10 and low silicon contents do not exhibit any diffraction signal at low angle, with the exception of SiTi-H10-10. These results can be attributed to hydrolysis and condensation reactions of Ti precursor being too fast for H = 10 to ensure a proper arrangement of the inorganic oxide around the surfactant micelles.

Figure 3 shows the DR-UV/Vis spectra registered as the Kubelka-Munk function, F(R), for all the SiTi-H3 samples. The initial absorption branch clearly shifts to shorter wavelengths when the silicon concentration is increased, this effect being especially intense for the highest Si/Ti molar ratio. Similar trends were detected for the series of samples prepared with higher water amounts. It has been reported that the inclusion of silicon atoms produces a disruption of the pure titania framework and delays its transition from amorphous to crystalline state [29]. In addition, for the mixed SiO_2-TiO_2 oxides with low titania concentrations, quantum effects due to the high dispersion of TiO_2 entities and/or the generation of titanium oxide species with low coordination numbers are the main responsible of this absorption change to shorter wavelengths.

The lower amount of valence electrons taking part in the electronic configuration of the material, caused by interruption of the structure by silicon atoms, leads to a larger energy gap between electronic bands and, consequently, the threshold wavelength for light absorption decreases (higher energy). In this way, band-gap (E_G) was calculated from the initial absorption branch of these spectra, the resulting values for all the samples being included in Table 3. In parallel to the shift of the threshold absorption to

shorter wavelengths, E_G moves to higher values as the silicon content of the xerogel is increased. Thus, while pure TiO_2 exhibits E_G values around 3.42 - 3.48 eV, this parameter changes to 3.77, 3.79 and 3.73 eV for the samples SiTi-H3-70, SiTi-H6-70 and SiTi-H10-70, respectively.

The titanium content of the mixed oxides was determined by Inductively Coupled Plasma (ICP) technique. Table 3 includes the results of such analysis, together with the theoretical value, both expressed as weight percent of Ti into the total mass of solid (TiO_2+SiO_2+humidity). Both real and theoretical values are very similar for the whole range of samples prepared, confirming the suitability of this synthesis procedure to carry out the hydrolysis and simultaneous condensation of both Ti and Si precursors.

Figure 4 shows the TEM images corresponding to a number of samples. A continuous and homogeneous porosity, without long-range order but with a typical wormhole-like structure, can be observed for all the samples, although those synthesized with H = 6 seem to have a better mesoscopic order.

Using the Energy Dispersion X-ray (EDX) accessory, integrated in the TEM equipment, local Si/Ti ratios were determined for several samples, the resultant values being registered in Table 3. Areas below 0.1 μm^2 belonging to different and thin particles were selected and analyzed. Thus, EDX analysis gives the chemical composition of the material in a microscopic level, so that the xerogel homogeneity can be checked. Figure 5 illustrates a typical EDX pattern, as well as the molar Si/(Ti+Si) percentage measured in 9 different particles of sample SiTi-H3-10. Cu and Cl signals can be observed, due to the sample holder and HCl used during the synthesis, respectively. Ti, Si and O atoms also appear, as it is expected for this sample. From the nine experimental data, an average molar Si/Ti ratio of 12.4/87.6 was determined, which is close to the theoretical

value (10/90). Moreover, the standard deviation is quite low, indicating both a high uniformity of the chemical composition and the absence of segregated phases.

Molar Si/Ti ratios of samples SiTi-H6-5, SiTi-H6-10, SiTi-H6-50 and SiTi-H10-10 were also determined by EDX technique, using the same procedure mentioned above. The mean resultant values were 5.9/94.1, 11.9/88.1, 52.1/47.9 and 13.6/86.4, respectively, with standard deviations of 0.1, 0.2, 1.7 and 3.21 respectively. Therefore, the occurrence of both a high efficiency for the silicon incorporation into the oxide framework and a good microscopic homogeneity for the three former samples can be concluded. However, a higher heterogeneity degree is observed for SiTi-H10-10 sample. As it has been commented previously, a high water concentration during the synthesis reactions increases the rate of hydrolysis and condensation reactions of the inorganic precursors, making more difficult to produce a good contact between the Si and Ti species and, consequently, to have a good dispersion of both atoms.

3.2 Thermal stability

Wide-angle XRD patterns were measured in-situ during nitrogen calcination up to 500 ºC of different mixed oxides using a high-temperature chamber. Figure 6 shows the patterns so obtained for the samples prepared with Si/Ti ratio = 10 and different hydrolysis molar ratios. For comparison, the same experiments were applied to the corresponding pure mesoporous TiO_2 materials. These last samples undergo a prompt transition from amorphous to anatase phase. Thus, for SiTi-H3-0 and SiTi-H6-0 samples a weak signal emerging at $2\theta \sim 25.35^{o}$, associated with (101) diffraction of such allotropic phase, can be observed when reaching a temperature of 178ºC. Indeed, the relatively high amount of acidic water employed for the synthesis reactions produces the crystallization of SiTi-H10-0 even during the aging step at 40ºC [21]. For pure TiO_2

samples, the diffraction peak becomes more intense and narrower as the temperature is increased, denoting a higher degree of crystallinity and larger crystal sizes, respectively. Neither rutile nor brookite phases were detected during the whole range of temperatures investigated (32-500ºC). While rutile is the thermodynamically stable crystalline phase of TiO_2, anatase is kinetically favoured. The selective formation of anatase has been previously reported for syntheses performed under the presence of chloride ions (HCl) [30, 31]. Since there is some amount of chloride ions remaining in each mixed oxide, coming from the synthesis step, they may be identified as responsible for this exclusive formation of anatase after calcination. Likewise, the mesoporous structure of pure TiO_2 samples may prevent the agglomeration and growth of titania units, keeping the crystallite size below the critical value required for the anatase to rutile transition [32,33].

Diffractograms of mixed oxides show that, in this case, the amorphous to anatase phase transition occurs at much higher temperatures. A low intense (101) diffraction peak of anatase can be detected at temperatures of 450, 400 and 350 ºC for SiTi-H3-10, SiTi-H6-10 and SiTi-H10-10, respectively, indicating that the threshold crystallization temperature decreases as the acidic water amount used during the synthesis reactions is higher. Similarly to pure mesoporous TiO_2 samples, this acceleration of the crystallization process is attributed to the generation of a larger number of surface reactive sites due to the hydrolysis and condensation reaction rates, which become faster as the hydrolysis molar ratio used in the synthesis step is increased. On the other hand, the interruption of TiO_2 framework with silicon atoms hinders the phase segregation during calcination and delays the crystallization temperature, confirming that this SiO_2 doping is a very effective method to stabilize mesoporous TiO_2-based materials.

The stabilization effect of silicon incorporation into titania matrixes has been already documented for different SiO_2-TiO_2 configurations: (a) TiO_2 nanoparticles dispersed into a SiO_2 matrix by the sol-gel method [34]; (b) coprecipitation of TiO_2 and SiO_2 from $TiCl_4$ and TEOS, respectively [18]; (c) supported SiO_2-TiO_2 films prepared by the sol-gel method [35] and (d) TiO_2 powders doped with Si through a sol-gel procedure [9]. In all cases, Si-O-Ti bonds were found to act as efficient barriers against sinterization and growth of TiO_2 particles. Thus, any crystallization process of TiO_2, either from amorphous to anatase phase or from anatase to rutile phase, was strongly delayed when silicon was incorporated into the titania matrix [18].

Table 4 lists the main textural properties, determined by N_2 (-196 °C) physisorption data, and the crystalline phase observed by XRD analysis, corresponding to different pure TiO_2 and SiO_2-TiO_2 porous materials after calcinations at 300 ºC during 3 h under static air. Although there is a clear reduction of both BET surface areas and pore volumes after calcination, these changes are remarkably more intense for silicon-free materials. For these samples, BET surface area drops are in the range 48.6 – 78.4 %, the final values being always close to 125 m^2/g. The percentage of lost surface area increases in the way SiTi-H10-0C < SiTi-H6-0C < SiTi-H3-0C. It is known that lower water contents during the synthesis stage lead to a lower polymerization degree of the TiO_2 framework, which usually results in higher BET surface areas and micropore volumes, as it has been previously demonstrated. However, this lower polymerization degree is associated to a higher surface reactivity generating higher porosity losses during calcination. Thus, microporosity is totally destroyed in the three pure titania samples after calcination. Mean pore size increases in all cases reaching values in the range 6.5-8.2 nm, whereas the corresponding BJH pore size distributions are still quite

narrow. This strong enlargement of the mean pore size is a clear indication of a structure collapse in pure TiO_2 materials as a consequence of the thermal treatment.

In contrast, porosity variations are less pronounced for SiO_2-TiO_2 materials, with final BET surface areas and mean pore diameters in the range 290-346 m^2/g and 3-3.9 nm, respectively, confirming a higher thermal stability. Moreover, a certain proportion of microporosity remains in all the mixed oxides. When comparing materials prepared with a Si/Ti = 10/90, the structural sensitivity to the temperature is found to increase with the hydrolysis molar ratio. In this way, the drop of BET surface area is 36.9 % and 22.6 % for H = 10 and 3, respectively. On the other hand, when the hydrolysis molar ratio is fixed to 6, it was observed that the higher silicon content, the higher thermal stability of the xerogel. Thus, while SiTi-H6-10 sample undergoes a loss of BET surface area of 29.9 %, SiTi-H6-20 presents a reduction of just 16 % in such parameter, its pore volume is almost constant and the enlargement of its mean pore size (from 2.2 to 3.0 nm) is the lowest registered among the whole set of samples here compared. These results point out the enhanced thermal stability of this sample.

Figure 7 displays the N_2 adsorption-desorption isotherms measured at -196 °C as well as the BJH pore size distribution corresponding to different SiO_2-TiO_2 porous mixed oxides before and after calcination at 300 ºC during 3 h. For comparison, the same analyses are plotted in Figure 8 for the equivalent pure mesoporous TiO_2 materials. It can be observed that calcination of pure titania xerogels produces a clear reduction in the adsorption at low relative pressures, this fact denoting a strong loss of microporosity and specific surface area, accompanied by a decrease in the total pore volume, as it can be appreciated from the lower nitrogen uptake at the highest relative pressures. Likewise, the hysteresis loop becomes more pronounced and shifted to higher relative

pressures, indicating a larger bottle-neck effect in the pore geometry and an enlargement of the mean pore size, as it can be also observed in the BJH graphs. On the contrary, the total pore volume of SiO_2-TiO_2 mixed oxides is practically not affected by the thermal treatment. A shift of the maximum of N_2 uptake in the BJH distribution to higher relative pressures is detectable, but in a milder way than for pure titania samples, denoting a significant stability of mesopores under the thermal treatment. Adsorption at low relative pressures drops after calcinations, indicating an important loss of microporosity, and an enlargement of the hystereris loop also occurs in this series of samples. From these results, it can be concluded that no collapse but a slight modification of the pore structure, probably due to a densification of the pore walls induced by the temperature, takes place for the mixed oxides. Therefore, they can be considered as thermally stable materials, at least in the temperature range here investigated.

Finally, Figure 9 represents the low-angle XRD patterns of the mixed oxides, before and after calcination at 300ºC during 3h. A single diffraction peak, denoting some short-range mesoscopic order, can be detected even for SiTi-H10-10C, although crystallization of its pore walls to anatase phase has taken place (Table 4). Furthermore, the diffraction peak becomes narrower after the thermal treatment for SiTi-H3-10C and SiTi-H6-10C, indicating that introducing small amounts of SiO_2 into the mesoporous titania framework not only enhances its thermal stability but also induces a better rearrangement of the pore structure under a mild calcination.

In summary, SiO_2-doping of micelle -templated TiO_2-based materials has shown to be a very effective method to obtain mesoporous solids having an enhanced pore ordering and thermal stability.

4. Conclusions

Mesoporous SiO_2-TiO_2 powders have been synthesized by the sol-gel route, using titanium tetraisopropoxide (TTIP) as TiO_2 precursor, tetraethylorthosilicate (TEOS) as SiO_2 precursor and triblock copolymer P-123 as structure directing agent, this surfactant being eliminated by ethanol extraction after the synthesis step. The results indicate that silicon atoms can be totally incorporated into the TiO_2 framework, giving materials with a very high dispersion and homogeneity for Si/Ti molar ratios ranging from 5/95 to 70/30.

Mixed oxides prepared with Si/Ti molar ratios of 50/50 represent a transition from materials with TiO_2 as the inorganic matrix to others with SiO_2 as the predominant phase, the gelation time, structural and porous properties being largely determined by this factor.

For low Si-loadings, it has been concluded that the silicon incorporation not only enhances the mesophase order, but also strongly improves the thermal stability of the mesoporous structure. Thus, for materials prepared with Si/Ti = 10/90, the transition of titania particles from amorphous to anatase phase is delayed from 178ºC up to 350 – 450ºC, depending on the hydrolysis molar ratio employed during the synthesis step. The disruption of the TiO_2 framework by Si-O-Ti bonds and the stabilization effect of the mesoporous structure against the sinterization process are proposed as the main responsible of such behaviour. Thus, while pure TiO_2 materials synthesized using the same conditions exhibit BET surface areas around 125 m^2/g after calcination at 300 ºC for 3h, SiO_2-TiO_2 mixed oxides containing Si/Ti ratios of 10/90 or 20/80 present S_{BET} values in the range 290-346 m^2/g. Moreover, the mesoscopic order seems to be enhanced after such thermal treatment. This fact, together with the selective

crystallization of TiO_2 nanoparticles of the pore walls to anatase phase, make these materials very promising for photocatalytic applications, where anatase nanocrystals (potentially with high photoactivity), high surface areas and uniform mesopore size (for a more effective anchoring of modifiers, such as dyes molecules in order to absorb visible light) are demanded.

Acknowledgments

The authors wish to thank "Comunidad de Madrid" for its financial support to the PHISICO2 Project through the Programme of Activities between Research Groups (S-0505/EN/0404).

References

[1] K.-N.P. Kumar, K. Keizer, A.J. Burggraaf, J. Mater. Chem. 3 (1993) 1141.

[2] K.C. Song, S.E. Pratsinis, J. Mater. Res. 15 (2000) 2322.

[3] J. Kim, K.Ch. Song, S. Foncillas, S.E. Pratsinis, J. Eur. Ceram. Soc. 21 (2001) 2863.

[4] B. Karmakar, D.Ganguli, Indian J. Technol. 25 (1987) 282.

[5] X. Ding, L. Liu, X. Ma, Z. Qi, Y. He, J. Mater. Sci. Lett. 13 (1994) 462.

[6] C. Anderson, A.J. Bard, J. Phys. Chem. B 10 (1997) 2611.

[7] S.R. Kumar, C. Suresh, A.K. Vasudevan, N.R. Suja, P. Mukundan, K.G.K. Warrier, Mater. Lett. 38 (1999) 161.

[8] X. Gao, I.E. Wachs, Catal. Today 51 (1999) 233.

[9] P. Cheng, M. Zheng, Y. Jin, Q. Huang, M. Gu, Mater. Lett. 57 (2003) 2989.

[10] K.M. Parida, S.K. Samantaray, H.K. Mishra, J. Colloid Interface Sci. 216 (1999) 127.

[11] R.W. Matthews, J. Catal. 113 (1988) 549.

[12] S. Takeda, S. Suzuki, H. Odaka, H. Hosono, Thin Solid Films 392 (2001) 338.

[13] N. Enomoto, K. Kawasaky, M. Yoshida, X. Li, M. Uheara, J. Hojo, Solid State Ionics 151 (2002) 171.

[14] R.B. Greegor, F.W. Lytle, D.R. Sandstrom, J. Wong, P. Schultz, J. Non-Cryst. Solids 55 (1983) 27.

[15] N. Hüsing, B. Launay, D. Doshi, G. Kickelbick, Chem. Mater. 14 (2002) 2429.

[16] C. Anderson, A.J. Bard, J. Phys. Chem. 99 (1995) 9882.

[17] R.F. de Farias, U. Arnold, L. Martínez, U. Schuchardt, M.J.D.M. Janini; C. Airoldi, J. Phys. Chem. Solids 64 (2003) 2385.

[18] S.M. Jung, O. Dupont, P. Grange, Appl. Catal. A 208 (2001) 393.

[19] A. Alvarez-Herrero, G. Ramos, F. del Monte, E. Bernabeu, D. Levy, Thin Solid Films 455-456 (2004) 356-360.

[20] K. Guan, Surf. Coat. Technol. 191 (2005) 155.

[21] G. Calleja, D.P. Serrano, R. Sanz, P. Pizarro, Ind. Eng. Chem. Res. 43 (2004) 2485.

[22] D. P. Serrano, G. Calleja, R. Sanz, P. Pizarro, Stud. Surf. Sci. Catal. 135 (2001) 251.

[23] G. J. de A. A. Soler-Illia, A. Louis, and C. Sanchez, Chem. Mater. 14 (2002) 750.

[24] T. Czuryszkiewicz, F. Kleitz, F. Schüth, M. Lindén, Chem. Mater. 15 (2003) 3704.

[25] J. Klaas, G. Schulz-Ekloff, N.I. Jaeger, J. Phys. Chem. B 101 (1997) 1305.

[26] Y. Wang, A. Suna, W. Mahler, R. Kasowski, J. Chem. Phys. 87 (12) (1987) 7315.

[27] D.C.M. Dutoit, M. Schneider, A. Baiker, J. Catal. 153 (1995) 165.

[28] S. Klein, S. Thorimbert, W.F. Maier, J. Catal. 163 (1996) 476.

[29] H. Yamashita, S. Kawasaki, Y. Ichihashi, M. Harada, M. Takeuchi, M. Anpo, J. Phys. Chem. B 102 (1998) 5870.

[30] K. Yanagisawa, J. Ovenstone, J. Phys. Chem. B 103 (1999) 7781.

[31] D.P. Serrano, G. Calleja, R. Sanz, P. Pizarro, J. Mater. Chem. 17 (2007) 1178.

[32] C.C. Wang, J.Y. Ying, Chem. Mater. 11 (1999) 3113.

[33] Y. Li, N.H. Lee, E.G. Lee, J.S. Song, S.J. Kim, Chem. Phys. Lett. 389 (2004) 124.

[34] R.N. Viswanath, S. Ramasamy, Colloids Surf. A 133 (1998) 49.

[35] C.F. Song, M.K. Lü, P. Yang, D. Xu, D.R. Yuan, Thin Solid Films 413 (2002) 155.

Table 1. Gelation time of SiO_2-TiO_2 samples as a function of the hydrolysis molar ratio [H = mol H_2O/mol (Ti+Si)] and silicon concentrations.

Sample	Molar Si/Ti	Molar H_20/Si	Molar H_20/Ti	Gelation time
		H=3		
SiTi-H3-0	0/100	--	3	> 6 h
SiTi-H3-5	5/95	60	3.16	> 6 h
SiTi-H3-10	10/90	30	3.33	> 6 h
SiTi-H3-20	20/80	15	3.75	> 6 h
SiTi-H3-50	50/50	6	6	< 3 h
SiTi-H3-70	70/30	4.3	10	> 10 h
		H=6		
SiTi-H6-0	0/100	--	6	< 4 min
SiTi-H6-5	5/95	120	6.32	< 4 min
SiTi-H6-10	10/90	60	6.67	< 4 min
SiTi-H6-20	20/80	30	7.5	< 4 min
SiTi-H6-50	50/50	12	12	< 4 min
SiTi-H6-70	70/30	8.6	20	> 5 h
		H=10		
SiTi-H10-0	0/100	--	10	Immediate
SiTi-H10-5	5/95	200	10.5	Immediate
SiTi-H10-10	10/90	100	11.1	Immediate
SiTi-H10-20	20/80	50	12.5	Immediate
SiTi-H10-50	50/50	20	20	< 1 min
SiTi-H10-70	70/30	14.4	33.3	> 1 h
SiTi-H10-100	100/0	10	--	no gelation

Table 2. Textural properties of SiO_2-TiO_2 samples prepared using different hydrolysis molar ratios (H) and silicon concentrations.

Sample	Molar H_20/Si	S_{BET} (m^2/g)	V_{PORE} (cm^3/g)	V_{MIC} (cm^3/g)	d_{PORE} (nm)
H=3					
SiTi-H3-0	--	582	0.342	0.144	2.4
SiTi-H3-5	60	582	0.377	0.090	2.8
SiTi-H3-10	30	420	0.236	0.105	2.3
SiTi-H3-20	15	396	0.210	0.112	2.4
SiTi-H3-50	6	98	0.036	0.036	< 2
SiTi-H3-70	4.3	275	0.107	0.107	< 2
H=6					
SiTi-H6-0	--	381	0.249	0.068	2.7
SiTi-H6-5	120	390	0.254	0.103	< 2 / 3.8
SiTi-H6-10	60	437	0.248	0.102	2.3
SiTi-H6-20	30	412	0.227	0.122	2.2
SiTi-H6-50	12	231	0.094	0.094	< 2
SiTi-H6-70	8.6	438	0.254	0.102	2.3
H=10					
SiTi-H10-0	--	245	0.252	0	4.1
SiTi-H10-5	200	459	0.312	0.118	2 / 4.2
SiTi-H10-10	100	460	0.280	0.132	2.6
SiTi-H10-20	50	515	0.271	0.157	2.0
SiTi-H10-50	20	340	0.154	0.149	< 2
SiTi-H10-70	14.4	276	0.113	0.113	< 2
SiTi-H10-100	10	420	0.179	0.179	< 2

Table 3. Composition and optical properties of SiO_2-TiO_2 samples prepared using different hydrolysis molar ratios (H) and silicon concentrations.

Sample	Molar H_20/Si	E_G (eV)	Ti content (wt.%) Theoretical	Ti content (wt.%) Experimental	Si/Ti by EDX	σ^2
			H=3			
SiTi-H3-0	--	3.48	--	--	--	--
SiTi-H3-5	60	3.63	44.4	47.2	--	--
SiTi-H3-10	30	3.56	42.0	42.7	12.4/87.6	0.877
SiTi-H3-20	15	3.57	39.8	38.2	--	--
SiTi-H3-50	6	3.65	25.9	28.8	--	--
SiTi-H3-70	4.3	3.77	16.6	15.8	--	--
			H=6			
SiTi-H6-0	--	3.48	--	--	--	--
SiTi-H6-5	120	3.51	43.8	48.5	5.9/94.1	0.1
SiTi-H6-10	60	3.59	42.6	45.6	11.9/88.1	0.2
SiTi-H6-20	30	3.57	39.9	41.6	--	--
SiTi-H6-50	12	3.64	26.1	28.4	52.1/47.9	1.7
SiTi-H6-70	8.6	3.79	16.9	18.1	--	--
			H=10			
SiTi-H10-0	--	3.42	--	--	--	--
SiTi-H10-5	200	3.53	44.1	43.0	--	--
SiTi-H10-10	100	3.60	42.2	39.2	13.6/86.4	3.21
SiTi-H10-20	50	3.60	38.4	39.4	--	--
SiTi-H10-50	20	3.66	26.2	25.9	--	--
SiTi-H10-70	14.4	3.73	16.8	16.3	--	--
SiTi-H10-100	10	--	--	--	--	--

Table 4. Characterization of SiO_2-TiO_2 samples after calcination at 300ºC for 3 h.

Sample	S_{BET} (m^2/g)	Loss of surface area (%)	V_{PORE} (cm^3/g)	V_{MIC} (cm^3/g)	d_{PORE} (nm)	Phase
SiTi-H3-0C	126	78.4	0.186	0	6.5	Anatase
SiTi-H6-0C	122	67.9	0.210	0	8.0	Anatase
SiTi-H10-0C	126	48.6	0.190	0	8.2	Anatase
SiTi-H3-10C	325	22.6	0.253	0.069	3.7	Amorphous
SiTi-H6-10C	306	29.9	0.249	0.066	3.7	Amorphous
SiTi-H6-20C	346	16.0	0.222	0.114	3.0	Amorphous
SiTi-H10-10C	290	36.9	0.258	0.099	3.9	Anatase

FIGURE CAPTIONS

Figure 1. N_2 (-196 °C) physisorption isotherms (A) and BJH pore size distributions (B) of SiO_2-TiO_2 porous materials prepared using H = 3 and different Si/Ti molar ratios.

Figure 2. Low-angle XRD patterns of SiO_2-TiO_2 porous materials prepared using different hydrolysis molar ratios and Si concentrations.

Figure 3. DR-UV/Vis spectra of SiO_2-TiO_2 porous materials prepared using H = 3 and different Si/Ti molar ratios.

Figure 4. TEM images of SiO_2-TiO_2 porous samples: (A) SiTi-H3-10; (B) SiTi-H6-10; (C) SiTi-H6-50 and (D) SiTi-H10-10.

Figure 5. EDX analysis of SiTi-H3-10 sample showing the percentage of Si atoms relative to total amount of Si+Ti, measured for different particles. Figure inside illustrates the EDX spectra obtained for one of these particles.

Figure 6. Wide-angle XRD pattern set corresponding to different SiO_2-TiO_2 and pure TiO_2 porous materials, measured in a high temperature chamber heating at different temperatures up to 500 ºC.

Figure 7. N_2 (-196 °C) physisorption isotherms (A) and BJH pore size distributions (B) of SiO_2-TiO_2 porous materials before and after calcination (labelled with C) at 300 ºC for 3 h.

Figure 8. N_2 (-196 °C) physisorption isotherms (A) and BJH pore size distributions (B) of pure TiO_2 porous materials before and after calcination (labelled with C) at 300 ºC for 3 h.

FIGURE 1

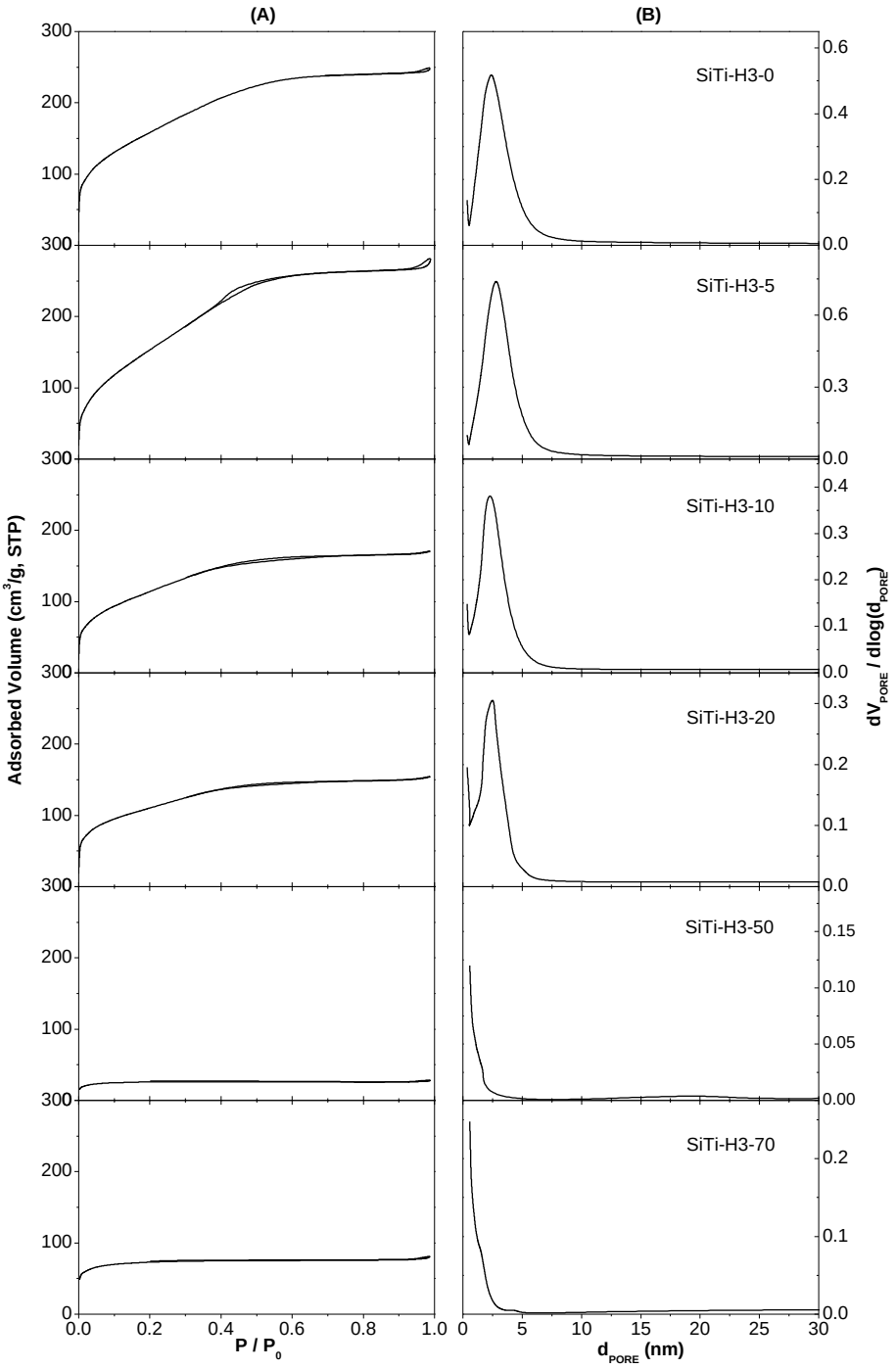
(A)
(B)
SiTi-H3-0
SiTi-H3-5
SiTi-H3-10
SiTi-H3-20
SiTi-H3-50
SiTi-H3-70
Adsorbed Volume (cm³/g, STP)
P / P0
dVPORE / dlog(dPORE)
dPORE (nm)

FIGURE 2

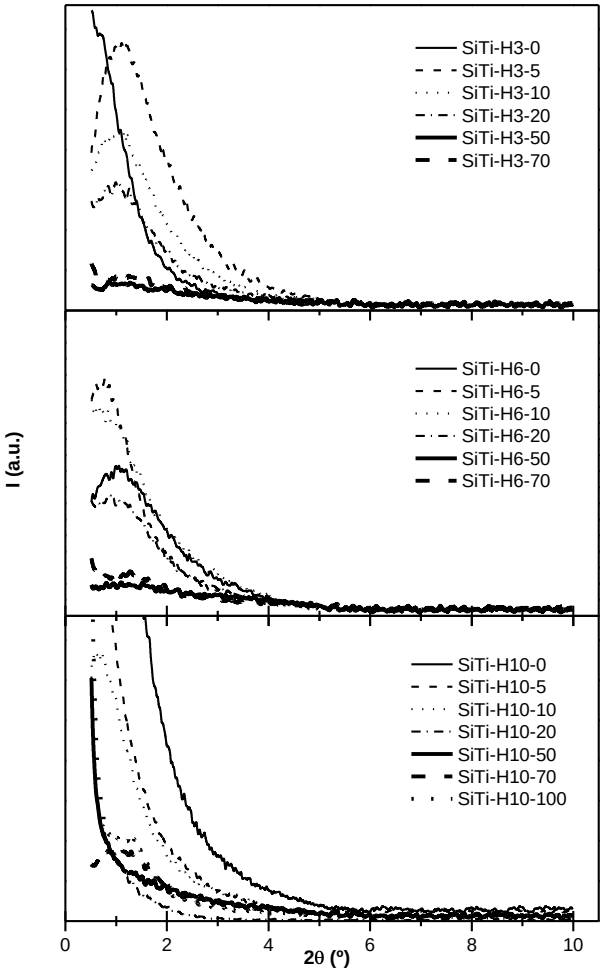
SiTi-H3-0
SiTi-H3-5
SiTi-H3-10
SiTi-H3-20
SiTi-H3-50
SiTi-H3-70
SiTi-H6-0
SiTi-H6-5
SiTi-H6-10
SiTi-H6-20
SiTi-H6-50
SiTi-H6-70
SiTi-H10-0
SiTi-H10-5
SiTi-H10-10
SiTi-H10-20
SiTi-H10-50
SiTi-H10-70
SiTi-H10-100
I (a.u.)
0
2
4
6
8
10
2θ (°)

FIGURE 3

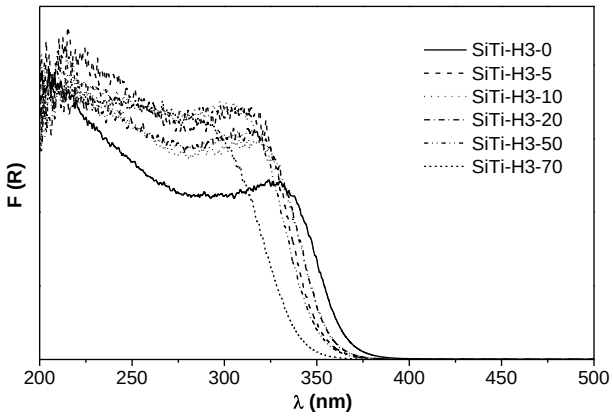
SiTi-H3-0
SiTi-H3-5
SiTi-H3-10
SiTi-H3-20
SiTi-H3-50
SiTi-H3-70
F (R)
200
250
300
350
400
450
500
λ (nm)

FIGURE 4

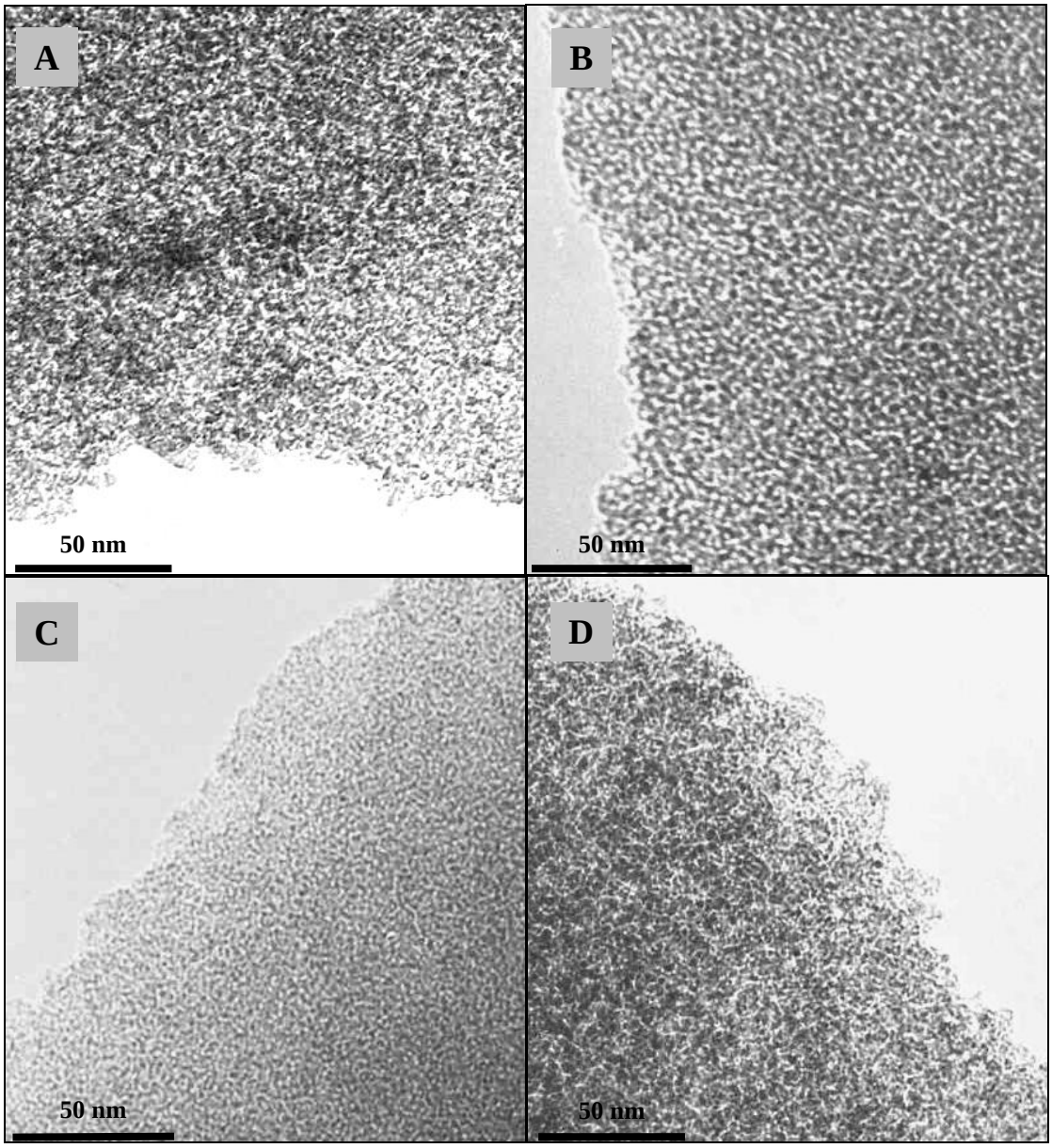

FIGURE 5

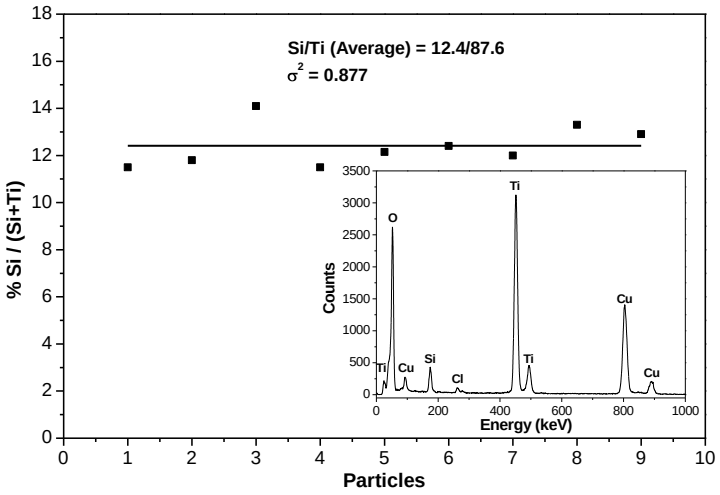
Si/Ti (Average) = 12.4/87.6
σ² = 0.877
% Si / (Si+Ti)
Particles
Counts
Energy (keV)
O
Ti
Cu
Si
Cl
Ti
Ti
Cu
Cu

FIGURE 6

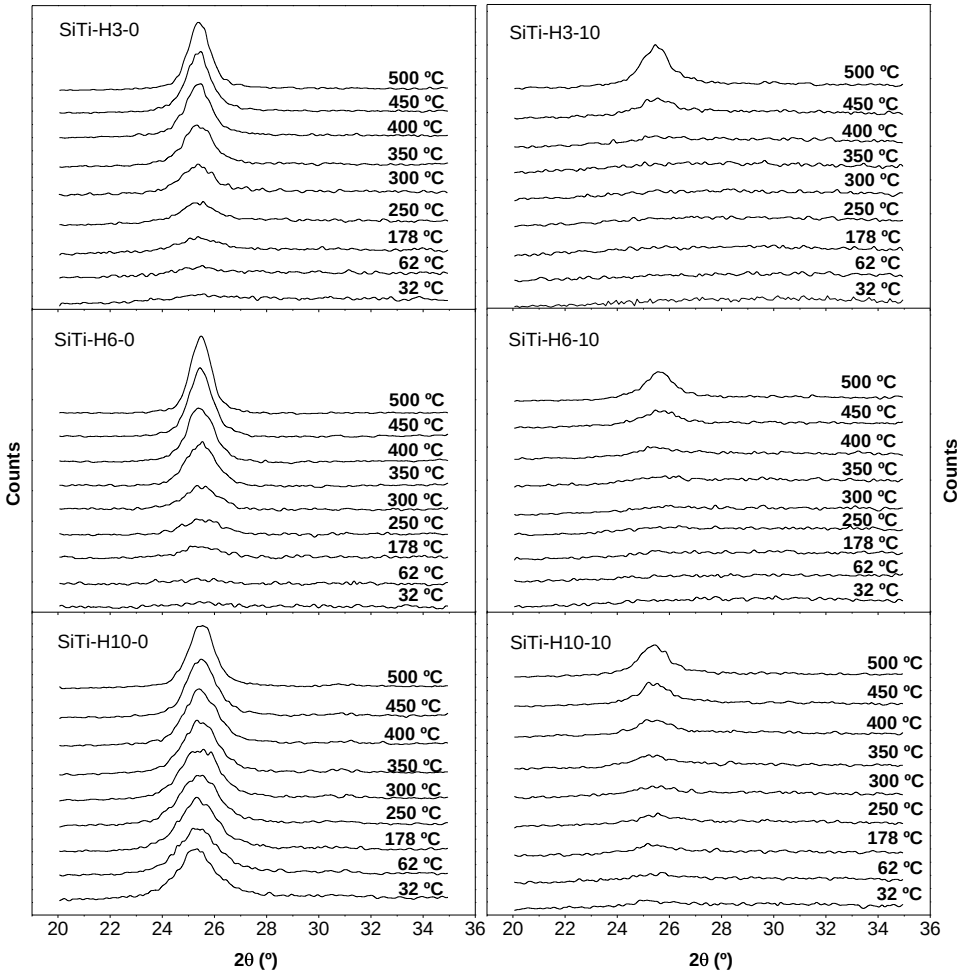
SiTi-H3-0
SiTi-H3-10
SiTi-H6-0
SiTi-H6-10
SiTi-H10-0
SiTi-H10-10
500 ºC
450 ºC
400 ºC
350 ºC
300 ºC
250 ºC
178 ºC
62 ºC
32 ºC
Counts
2θ (º)
20
22
24
26
28
30
32
34
36

FIGURE 7

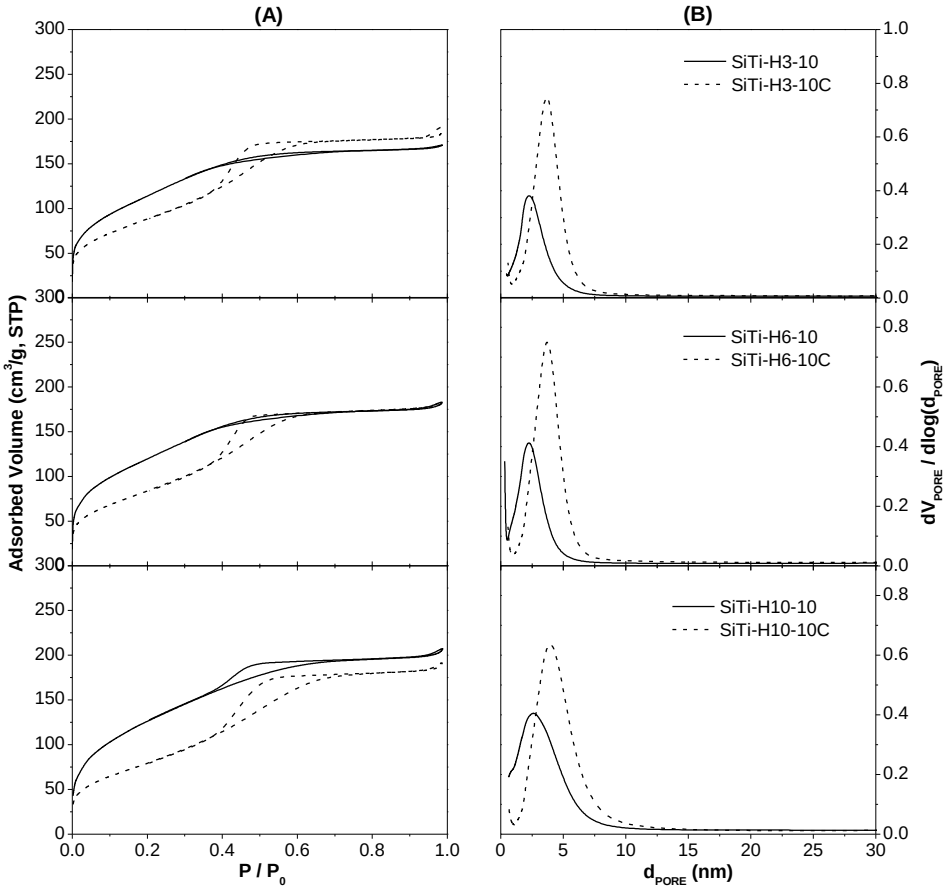
(A)
(B)
Adsorbed Volume (cm³/g, STP)
P / P0
dVPORE / dlog(dPORE)
dPORE (nm)
SiTi-H3-10
SiTi-H3-10C
SiTi-H6-10
SiTi-H6-10C
SiTi-H10-10
SiTi-H10-10C

FIGURE 8

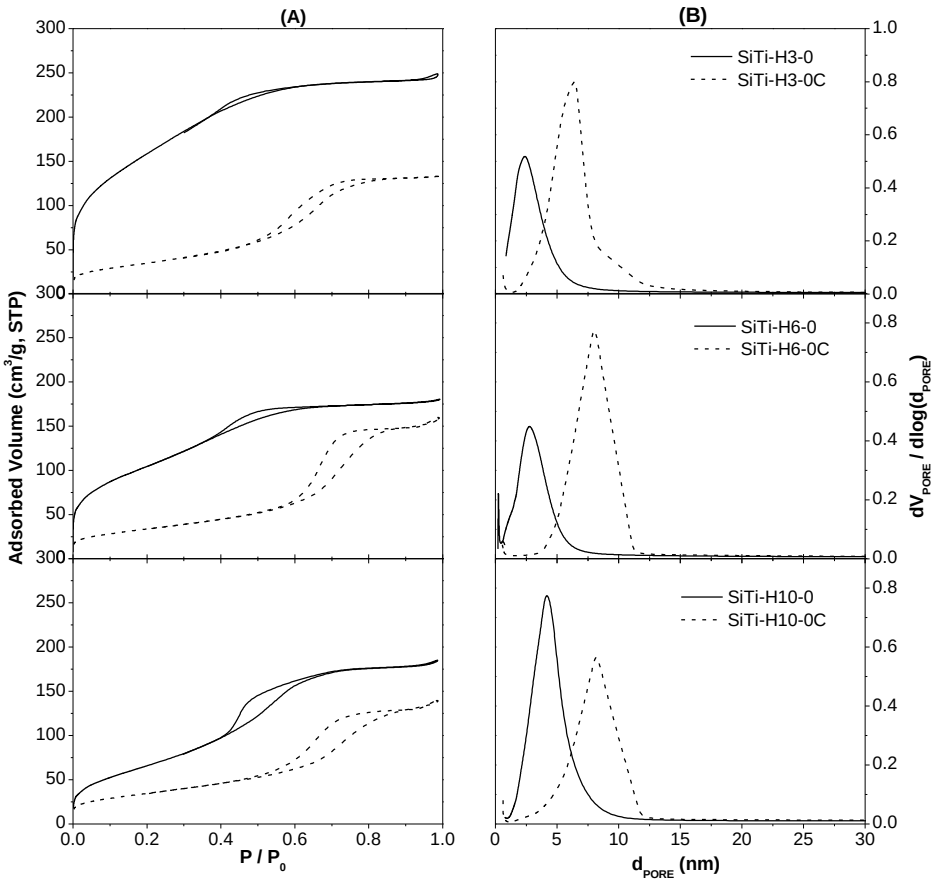
(A)
(B)
Adsorbed Volume (cm³/g, STP)
P / P0
dVPORE / dlog(dPORE)
dPORE (nm)
SiTi-H3-0
SiTi-H3-0C
SiTi-H6-0
SiTi-H6-0C
SiTi-H10-0
SiTi-H10-0C

FIGURE 9

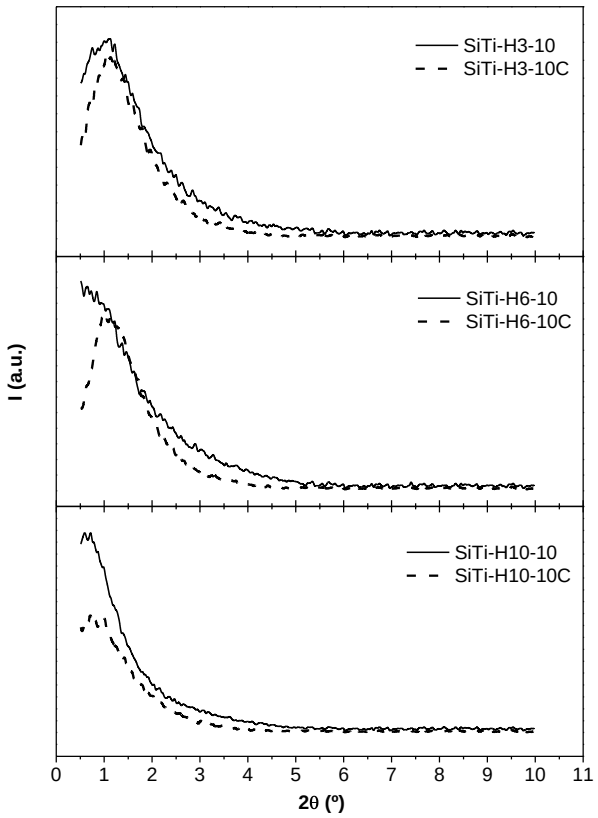
SiTi-H3-10
SiTi-H3-10C
SiTi-H6-10
SiTi-H6-10C
SiTi-H10-10
SiTi-H10-10C
I (a.u.)
0
1
2
3
4
5
6
7
8
9
10
11
2θ (º)